

Automatic Transfer Function Specification for Visual Emphasis of Coronary Artery Plaque

S. Glaßer¹, S. Oeltze¹, A. Hennemuth², C. Kubisch¹, A. Mahnken³, S. Wilhelmsen⁴ and B. Preim¹

¹Department of Simulation and Graphics, University of Magdeburg, Magdeburg, Germany

²Fraunhofer MEVIS, Bremen, Germany

³Department of Radiology, University Hospital, Magdeburg, Germany

⁴Department of Radiology, University Hospital, Aachen, Germany

Abstract

Cardiovascular imaging with current multislice spiral computed tomography (MSCT) technology enables a non-invasive evaluation of the coronary arteries. Contrast-enhanced MSCT angiography with high spatial resolution allows for a segmentation of the coronary artery tree. We present an automatically adapted transfer function (TF) specification to highlight pathologic changes of the vessel wall based on the segmentation result of the coronary artery tree. The TFs are combined with common visualization techniques, such as multiplanar reformation and direct volume rendering for the evaluation of coronary arteries in MSCT image data. The presented TF-based mapping of CT values in Hounsfield Units (HU) to color and opacity leads to a different color coding for different plaque types. To account for varying HU values of the vessel lumen caused by the contrast medium, the TFs are adapted to each dataset by local histogram analysis. We describe an informal evaluation with three board-certified radiologists which indicates that the represented visualizations guide the user's attention to pathologic changes of the vessel wall as well as provide an overview about spatial variations.

Keywords: transfer function, volume rendering, vessel visualization

ACM CCS: I.3.3 [Computer Graphics]: Display algorithms

1. Introduction

Coronary artery disease (CAD) is the leading cause of death in western nations [Ame07]. For CAD diagnosis, several image modalities are applied, for example, conventional invasive X-ray angiography, computed tomography (CT) of the heart and the coronary artery tree or optical coherence tomography for individual characterization of atherosclerotic CAD [FDHL03]. Multislice spiral CT (MSCT) allows for a high spatial resolution with short acquisition times. For enhancement of the blood, contrast agent is applied. With non-invasive contrast-enhanced CT coronary angiography (CTA), CAD can be reliably excluded. Thus, especially for asymptomatic patients with a high CAD risk (due to increased blood pressure, age, gender and stress), CTA is the image modality of choice. Since CTA allows for an assessment of the vessel's cross-sectional area, it has great potential for non-

invasive identification, characterization, and quantification of atherosclerotic CAD [HZZ*07]. Atherosclerotic CAD is the result of accumulations in the coronary artery wall, so-called plaques. Plaque deposits are small structures with inhomogeneous densities inside the vessel wall. Due to varying HU values and the non-uniform contrast agent accumulation, not all plaques can be segmented directly in CTA data. A visual emphasis of plaque should take the varying HU values into account and has to be adapted to each dataset.

We present an automatically adapted transfer function (TF) specification for the qualitative evaluation of CTA datasets. Because the coronary artery vessel wall and its pathologic changes have a small extent in comparison to the whole CTA dataset, global histogram analysis is not sufficient for the TF specification. Therefore, our approach is based on a coarse segmentation of the coronary artery tree and local

histogram analyses of the segmentation result. The adapted TF allows for the visualization of the coronary vessel wall and highlighting of plaques. Furthermore, the TF is combined with common visualization techniques for CAD evaluation in CTA data, that is maximum intensity projection (MIP), multiplanar reformation (MPR), curved multiplanar reconstruction (CPR) [KFW*02] for 2D views, and direct volume rendering techniques (DVR) for 3D views.

2. Medical Background

In this section, we provide additional information about the medical background of atherosclerotic plaque. Plaque deposits in the coronary artery vessel wall contain different accumulations, i.e. lipid or fibrous tissue, and can be classified into soft, fibrous and hard plaques. The lipid-rich soft plaques are prone to rupture and thus very dangerous for the patient. For individual soft plaque characterization, imaging modalities such as OCT can be employed. Fibrous plaques and hard plaques consist of more dense accumulations and are estimated to be more stable. In addition, hard plaque deposits contain calcium accumulations and thus are also referred to as calcified plaques. The overall coronary calcium acts as an indicator for the patient's whole plaque burden. For the detection and quantification of the coronary calcium, non-enhanced MSCT is primarily employed. Quantification is carried out by applying calcium scores to the data, e.g. the Agatston score [AJH*90]. The Agatston score defines a threshold for hard plaques as the sum of the mean plus twice the standard deviation of the non-enhanced blood intensity.

In CTA datasets, the contrast agent allows for a better depiction of the blood. Thus, a detection of stenoses and corresponding plaque types is possible. A stenosis is a narrowing of the lumen – the vessel's inner open area. Since a reliable exclusion of CAD based on CTA is possible, it has been established for asymptomatic patients, patients with abnormal coronary spatial variation or ambiguous medical test results. Furthermore, it is employed for the monitoring of coronary stents. Stents are artificial support devices, for example stainless steel mesh tubes, that are placed in a coronary artery after CAD treatment to keep the vessel open.

The early stages of atherosclerotic CAD do not necessarily lead to significant stenoses, since they can be compensated by a positive remodeling of the vessel wall, see Figure 1. Therefore, the evaluation of the coronary artery lumen is insufficient for the assessment of the patient's plaque burden, and the pathologic change of the vessel wall has to be taken into account. Evaluation of the lumen and the vessel wall is carried out in 2D MPR and CPR views. Oblique MPRs enable a cross-sectional view of the coronary artery and its wall along the vessel's centerline, whereas CPRs provide the vessel's longitudinal view [KFW*02]. DVR techniques convey information on the complex anatomy of the entire coronary tree. However, these visualizations provide only

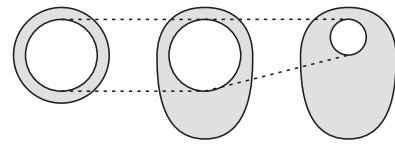


Figure 1: Illustration of remodeling in cross-section views. Left, a normal vessel wall (gray) is depicted. Early stages of CAD are compensated by positive remodeling—an increasing wall thickness (center). Negative remodeling, caused by progressive CAD, yields a stenosis (right).

limited information about pathologic vessel wall changes and the coronary artery lumen.

3. Related Work

A large variety of techniques for the visualization of vasculature exists, which can be grouped into surface rendering (SR) and DVR approaches. SR relies on the extraction of vascular structures, e.g. by thresholding or explicit segmentation, which is followed by the conversion into a polygonal mesh, see [PO07] for an overview. For the evaluation of CAD, we consider that SR is not appropriate, since the vessel wall and possible small inhomogeneous plaque deposits inside are likely to be too small for reliable extraction. Therefore, SR of CTA data would convey an accuracy, which does not correspond to the underlying data. Furthermore, transitions in the TF domain may not be represented with SR. Thus, we chose DVR, as has been suggested in [vOvGR*03].

With DVR, the indirect classification of surfaces of interest is carried out by employing TFs. Special approaches exist to support the interactive TF definition for different applications [KKH02]. The drawback is the considerable inter-observer variability, which affects the derived interpretation. Rezk-Salama *et al.* [RSK06] employ a layer technique that applies simple TFs to reveal inner structures. Hence, accuracy was less important than interactivity, which does not hold for CAD diagnosis. We aim at an automatically defined TF as starting point for further exploration. In addition to image data values, derived information such as gradient magnitude [KKH02] or distance to some reference structure [TPD06] can be employed yielding multidimensional TFs. Gradient-based TFs can improve the boundary enhancement between blood pool and surrounding tissue, but no improvement could be achieved for the visualization of the vessel wall itself and its inner structures due to the small extents and thus high sensitivity to noise and artefacts. Since the remodeling of the vessel wall leads to varying lumen diameters, we do not employ distance-based TFs. Correa *et al.* [CM08] applied scale fields for size-based TF generation and Vega *et al.* [VST*03, VST*04] discussed the automatic 2D TF design to emphasize vascular structures based on intensity values and gradient magnitude. Another method was

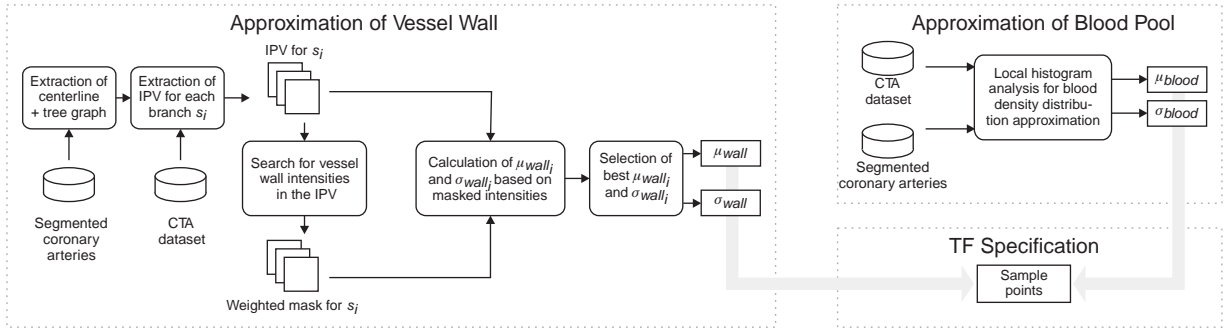


Figure 2: Schematic overview of automatic approximation of the parameters μ_{blood} , σ_{blood} , μ_{wall} and σ_{wall} for the TF specification. The parameters of the blood are calculated by local histogram analysis of the segmented coronary artery tree (top right). For the vessel wall intensity approximation, μ_{wall} and σ_{wall} are chosen from a set of μ_{wall_i} and σ_{wall_i} for all coronary artery branches b_i (left). First, the centerline of the coronary tree segmentation is extracted and branches are identified. Second, for each branch b_i , an intensity profile volume (IPV) is extracted. Based on the IPV, a weighted mask for vessel wall intensities is determined and applied to the IPV to obtain a sample set of vessel wall intensities, from which μ_{wall_i} and σ_{wall_i} can be extracted.

presented by Joshi *et al.* [JQD*08]. They emphasize vasculature by employing a non-parametric vessel detection method, which works well even at branchings. Although these approaches allow for highlighting of vasculature, they do not emphasize abnormalities in the vessel wall. Our concept is similar to [LLY05], who employ local histogram analyses to differentiate between organ tissues.

In general, different views are combined for CAD evaluation in CTA data, as presented in [KHB*06] and [SCC*04]. In both approaches, DVR provide spatial information, whereas the more detailed vessel evaluation is carried out in the 2D CPR or MPR views. Other imaging methods for vascular structures are maximum intensity projection (MIP), for example the MIP views of segmented objects [BA02], sliding thin-slab MIPs [NRJ93] and the novel maximum intensity difference accumulation (MIDA) approach, where shape cues are provided [BG09].

For the separation of calcified hard plaques, Isgum *et al.* [IRvG07] introduced an approach for non-enhanced CT. For CTA data, Hong *et al.* [HBS*02] applied calcium scores, yielding a threshold of 350 HU for hard plaque separation. Wesarg *et al.* [WFKF06] detected hard plaques in CTA data by analyzing the minimal diameter of the vessel lumen and examining stenotic regions. Moreover, they presented a simultaneous mapping of the minimal lumen diameter to color and to the diameter of a tube around the vessel for highlighting of stenoses. The automatic detection and separation of soft and fibrous plaques is difficult because clinical studies reveal different and sometimes overlapping HU intervals for these plaque types in CTA data [PAM*07].

4. Concept

We present an automatic TF specification for visual emphasis of soft and fibrous plaques and for a visual separation

of hard plaques and coronary stents. In contrast to conventional methods, we highlight the vessel wall instead of the contrast-enhanced lumen of the coronary arteries, including stenotic and non-stenotic plaques. The TF specification is carried out by determining supporting points, which depend on the mean intensity and standard deviation of the bloodpool (μ_{blood} , σ_{blood}) and the vessel wall (μ_{wall} , σ_{wall}).

Because the vessel wall and its pathologic changes cannot be discriminated in a global histogram, a segmentation method has to be employed, on which further analysis steps are based. We segment the coronary artery tree of a CTA dataset with the method described in [HBF*05]. The method was successfully tested for 61 datasets that were acquired with different CT scanners from healthy patients, patients with CAD and with anatomical abnormalities. These datasets also contained artefacts or inhomogeneous contrasts. During the segmentation process, branches of the coronary tree that were not detected in the initial segmentation can be interactively added by the user.

In this section, the automatic parameter extraction, based on the segmentation result, is described and followed by the TF specification. In Figure 2, an overview of the different steps is provided. At the end of this section, the volume rendering method for the 3D image display is described.

4.1. Approximation of the blood intensity distribution

For the approximation of the blood intensity distribution and thus the parameters μ_{blood} and σ_{blood} , a local histogram analysis is applied to the segmented coronary artery tree, since the segmentation result mainly contains voxels representing the contrast-enhanced blood. Due to other intensities originating from surrounding tissue or interpolation issues, the parameters μ_{blood} and σ_{blood} cannot be directly derived from the local histogram.

CT data acquisition is known to be subject to noise with a Gaussian distribution where the noise level depends primarily on the amount of ionizing radiation (higher radiation leads to a better signal-to-noise ratio). Assuming a Gaussian distribution of the intensity values, we estimate its parameters μ and σ by determining an optimal fit to the intensity distribution to the local histogram of all segmented voxels. The fit is carried out by employing a least square method and binary search methods. Results for μ_{blood} and σ_{blood} indicate that the average intensity of the blood strongly differs for each tested dataset (i.e. $\mu_{blood} = 356HU \pm 136HU$ and $\sigma_{blood} = 46HU \pm 16HU$ for all tested datasets). Thus, a static threshold for all datasets for the separation of hard plaques, for example 350 HU suggested by Hong *et al.* [HBS*02], from contrast-enhanced blood is not applicable.

For hard plaque separation, we experienced an overestimation by applying a threshold as presented by Agatston *et al.* [AJH*90] for the computation of the Agatston score, that is a threshold as the sum of the average plus twice the standard deviation of the approximated blood intensity distribution. Overestimation may arise due to artefacts or contrast medium accumulations in smaller branches.

To reduce overestimation, a higher threshold t , has to be determined. In combination, t has to be as small as possible, since even smaller hard plaques should be highlighted. We employ the number of skeleton voxels, with intensities larger than t as a criterion. Since hard plaques are contained in the vessel wall and not in the lumen, we assume that as few as possible centerline voxels should be masked by t . The factor 3 is the smallest whole-number multiple which allows for hard plaque separation and masks no more than 5% of the skeleton voxels. Therefore, we compute t as

$$t = \mu_{blood} + 3\sigma_{blood}. \quad (1)$$

In Section 5.2, we will discuss how sensitive t is to small changes.

Coronary stents, which are in general made of stainless steel mesh tubes, exhibit similar x-ray attenuation coefficients as hard plaques and will be highlighted in the same manner.

4.2. Approximation of the vessel wall intensity

The described method for blood intensity approximation is not applicable for the vessel wall, since the intensities of the vessel wall can neither be separated in a local histogram nor in a global histogram of the segmentation result due to the small number of vessel wall voxels. Therefore, we employ a local histogram analysis for each coronary artery branch (see Figure 2). To identify these branches, the centerline of the segmented coronary artery tree is generated. We employ a successive erosion of border voxels, also taking anisotropic voxel extents into account, to preserve the topology of the

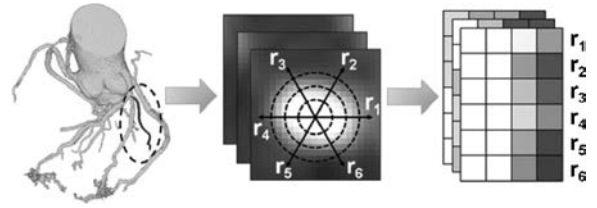


Figure 3: Extraction of the IPV. For each voxel of the local centerline of a coronary branch (left), n (e.g. 6) rays perpendicular to the centerline are casted (middle). Along the rays, intensities are sampled and stored in a slice of the IPV (right). Repeating this procedure for each centerline voxel of the branch yields the complete IPV.

initial mask, as it was presented by Selle *et al.* [SPSP02]. The centerline is transferred into a primitive tree graph representation, where each branch consists of a list with the corresponding centerline voxels and is linked to adjacent branches.

The local histograms for the vessel intensity approximation are generated by the intensity profile volume (IPV) extraction for each branch of the centerline. For each centerline voxel of a given branch, n rays perpendicular to the local centerline are cast and sampled in the CTA dataset. The number n of rays can be manipulated, depending on the voxel size and the diameter of coronary arteries, which tapers down from 5 mm to 1 mm. We empirically determine an amount of 16 rays for each tested dataset (with voxel size of $\approx 0.3 \text{ mm} \times 0.3 \text{ mm} \times 0.4 \text{ mm}$). A step size of half of the smallest voxel extent is sufficient for sampling. The rays are sampled for a certain distance. We recommend 3 mm to assure that the whole cross-section is sampled, since 2.5 mm is the maximum radius of coronary arteries. The sampled intensities are stored in a slice of the IPV (see Figure 3). By repeating this procedure for all centerline voxels, an IPV with a slice number that equals the number of centerline voxels is created.

In the next step, we detect the vessel wall intensities in the IPV. Since sampled intensities, which exhibit the same distances to the centerline voxel will appear as verticals in the IPV slice for this voxel, intensities representing the vessel wall will also be arranged in a vertical order. Therefore, we employ a slicewise search for vertical structures to the IPV. These verticals can be heavily distorted due to the approximation of the branch's real centerline with the branch of the centerline of the segmentation result, coronary artery wall remodeling, as well as artefacts arising from dense structures such as hard plaques, see Figure 4.

Vertical structures can be enhanced by a slicewise convolution of the IPV with a Laplacian of Gaussian (LoG) filter. Due to its small size, the partial volume effect has a strong influence on the vessel wall. Therefore, the LoG filter with

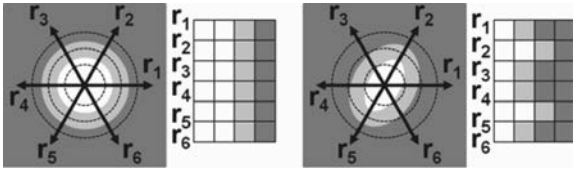


Figure 4: Schemes of cross-sectional vessel views. The casting of rays with the origin at the centerline in contrast-enhanced lumen (white) across the vessel wall (light gray) to surrounding tissue (dark gray) is illustrated. Ideally, circle-like cross-sections yield a vertical in the corresponding IPV slice (left), whereas ellipsoidal cross-sections lead to distorted vertical structures (right).

kernel size 3×3 first smooths the data of the IPV slice and then approximates the gradient magnitude. In the next step, a slicewise normalization and thresholding removes intensities with small gradient magnitudes. We employ a threshold of 0.5 for the normalized slices, which yields a binary mask that marks all intensities with a higher gradient magnitude. For taking also distorted vertical structures into account, we apply a weight function f_w to the voxels of each binary mask slice:

$$f_w = \begin{cases} 0 & \text{if } \frac{\sum \text{column}}{n} < 0.5 \\ \frac{\sum \text{column}}{n} & \text{else} \end{cases} \quad (2)$$

where n is the length of each column, that is the number of rays that were casted, and $\sum \text{column}$ is the number of fields with a normalized gradient magnitude > 0.5 . Due to distorted structures, it may occur that some slices of the weighted binary mask do not contain any value > 0 in special cases. These slices will be balanced by other slices containing non-zero weights. The sample set of the vessel wall intensities is obtained by employing the f_w -weighted binary mask to the original IPV yielding intensities d_i with weights w_i . Thus, w_i is the sum of all weights assigned by f_w to the density d_i .

For each branch b_i of the coronary artery tree, we determine μ_{wall_i} and σ_{wall_i} as the weighted arithmetic mean and the weighted arithmetic standard deviation of the remaining intensities of the sample set (see Figure 5). We then consider the branch b_i with the longest centerline and the parameters μ_{wall_i} and σ_{wall_i} that fulfill the condition $\mu_{\text{wall}_i} < \mu_{\text{blood}} - 2\sigma_{\text{blood}}$, as best candidate for the global vessel wall approximation. For all tested datasets, μ_{wall} was in the interval $[50HU, 270HU]$. The parameter extraction took in average ≈ 4 min for each dataset and was carried out on a 3.06 GHz processor with 3 GB of RAM.

Further analyses for other centerline branches reveal a trade-off between variability and quality. On the one hand, the variability of the spatial diffusion of the contrast agent causes

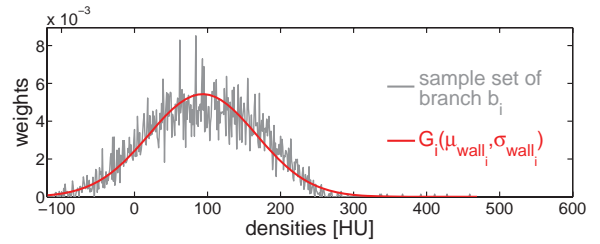


Figure 5: Sample set of an example branch b_i and the approximated Gaussian distribution with μ_{wall_i} and σ_{wall_i} .

different average intensity values for the approximation of the vessel wall, and thus local TFs should be generated. On the other hand, smaller branches are very sensitive to the partial volume effect. In addition, the centerline of the segmentation may be slightly off-centre for smaller branches, and these branches may exhibit too few voxels for a reliable estimation of μ_{wall} and σ_{wall} from the IPV, which results in poor quality. For example, the tested datasets exhibit strong differences even for the first two longest branches, that is the average difference of $\mu_{\text{wall}} \approx 63$ HU. In conclusion, no reliable visual improvements could be achieved with the employment of different local TFs, extracted with the proposed method.

4.3. TF specification

The automatic TF specification for the visualization of the coronary tree is based on supporting points, which only depend on μ_{wall} , σ_{wall} , μ_{blood} and σ_{blood} . For each supporting point, an opacity and a color value is assigned. Between these supporting points, opacities and colors are linearly interpolated. Basically, all TFs which highlight the vessel wall intensities and provide a visual separation of hard plaques and thus intensities larger than $t = \mu_{\text{blood}} + 3\sigma_{\text{blood}}$ will be considered as sufficient. Two more requirements should be fulfilled. First, full transparency should be assigned to the surrounding tissue and the contrast-enhanced blood. Second, to reveal inner structures, the vessel wall's intensities should be visualized transparently.

Color assignment to the supporting points aims at visual separation of hard plaques and stents and high contrasts for the vessel wall visualization. Because hard plaques and stents are very dense structures, they usually appear white or light gray in conventional gray scale CTA views. Therefore, intuitive visual separation is achieved by employing colors from beige to white in combination with high opacity values. For the vessel wall, a color scale from blue over red to green should be applied, yielding high contrasts for the visualization of different vessel wall intensities and thus different plaque deposits. Furthermore, low contrast between the vessel's outer boundary and surrounding tissue is necessary, since a reliable, precise segmentation of the whole

Table 1: Supporting point calculation for TF_{3D} and TF_{2D} . S_6 is the supporting point for hard plaque separation and thus identical to the threshold t , see Equation (1).

TF_{3D}		TF_{2D}	
S_0	$-1024HU$	S_0	$-1024HU$
S_1	$S_3 - \sigma_{wall}$	S_1	$S_3 - 2\sigma_{wall}$
S_2	$S_3 - \frac{1}{4}\sigma_{wall}$	S_2	$S_3 - \sigma_{wall}$
S_3	μ_{wall}	S_3	μ_{wall}
S_4	$S_3 + \frac{1}{4}\sigma_{wall}$	S_4	$\frac{1}{2}(S_3 + S_5)$
S_5	$\mu_{blood} - 2\sigma_{blood}$	S_5	$\mu_{blood} - 2\sigma_{blood}$
S_6	$\mu_{blood} + 3\sigma_{blood}$	S_6	$\mu_{blood} + 3\sigma_{blood}$
S_7	$S_6 + \sigma_{blood}$	S_7	$S_6 + \sigma_{blood}$
S_8	$3071HU$	S_8	$3071HU$

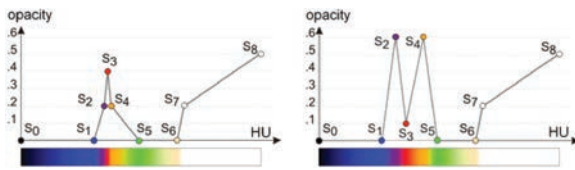


Figure 6: Graphs of the TF_{3D} (left) and TF_{2D} (right). Specification is carried out by calculation of μ_{wall} , σ_{wall} , μ_{blood} and σ_{blood} and thus the supporting points S_0 – S_8 . Between the points, optical properties are linearly interpolated. The x-axis is not labeled, since the HU values differ from dataset to dataset.

coronary artery vessel wall is absent due to its small extent. A high contrast discontinuity in the TF would imply too much accuracy on the exact location of the wall.

We define two TFs depending on the dimensionality of the viewer: the TF_{2D} and the TF_{3D} . To avoid occlusions in the 3D case, we employ the interval size $\mu_{wall} \pm \sigma_{wall}$ for the TF_{3D} and $\mu_{wall} \pm 2\sigma_{wall}$ for the TF_{2D} . We present one (of potentially several) solutions to our requirements by defining nine sample points S_0 – S_8 (see Table 1 and Figure 6).

The assignment of opacity values was compared to MIP views and the MIDA approach, recently presented by Bruckner *et al.* [BG09]. There was no clear improvement of the visualization of hidden structures with MIP or MIDA views, since the higher transparency of the vessel wall reveals occluded hard plaques in the TF_{3D} -based views. Furthermore, the low overall maximum opacity value, the small spatial extent of hard plaques and the local opacity changes from blood intensities to hard plaques and from surrounding tissue to the vessel wall, avoid the problem of an occlusion of a local maximum opacity change as discussed in [BG09].

While in DVR visualization the TF_{3D} is solely applied, in the 2D CPR and MPR views the TF_{2D} can be combined with a standard gray scale visualization. As no occlusion occurs

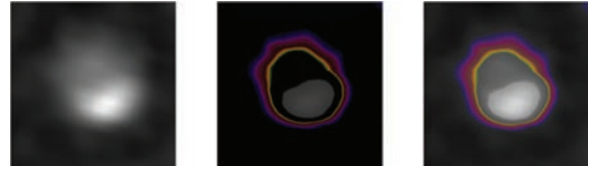


Figure 7: Combination of the windowing TF and the TF_{2D} by blending. On the left, the MPR view with a hard plaque (white area) is visualized by employing windowing. In the middle, the TF_{2D} was applied and on the right, the combination of TF_{2D} and windowing TF is presented.

in the 2D views, the TF_{2D} is overlaid by a conventional slice view to highlight the vessel wall and to provide contextual information of the unmasked data. The lookup table of the windowing TF is therefore blended, that is linearly interpolated, with the lookup table of the TF_{2D} , and the opacity value determines the influence of the TF_{2D} (see Figure 7). The user can manipulate the windowing TF's parameters and thus directly influence brightness and contrast of the combined TF_{2D} .

The automatically adapted global TFs allow for a qualitative evaluation of the CTA datasets. To improve exploration, the user can slightly change the automatically generated TFs. Therefore, an offset for the visual separation of hard plaques, that is S_6 , and for average vessel wall intensity, that is S_3 , can be manipulated, with the supporting points S_2 , S_4 and S_7 being updated accordingly. Manipulation may be necessary to cope with artefacts in smaller branches of selected datasets and allows for quality judgment. The user manipulation and thus the influence of the incrementally manipulated TFs is discussed in Section 5.

4.4. Rendering of the 3D DVR view

The display of the volume data, employing the TF_{3D} , was realized via GPU-raycasting. For the implementation, general setups and acceleration strategies, as described in [SHN*06] and [EKE01], were applied. Since the relevant volume resolution in the clinical routine is typically below $512 \times 512 \times 512$, the data easily fits in today's consumer graphics cards even with 16-bit float precision.

The renderer was implemented with the Luxinia 3D engine (www.luxinia.de), which is scriptable via Lua and uses OpenGL and Cg as rendering backend. Seven seconds are needed from application start to the first visible rendered frame and the achieved frame rate is ≈ 50 Hz. High quality shots with eight time finer ray steps are rendered when no interactions are performed and take less than 0.1 seconds. To raise the image quality with wider ray steps during interactive camera/object manipulation, we employ pre-integrated volume rendering from [EKE01]. The application was run at 1024×768 on a GeForce 9600 GT 512 MB.

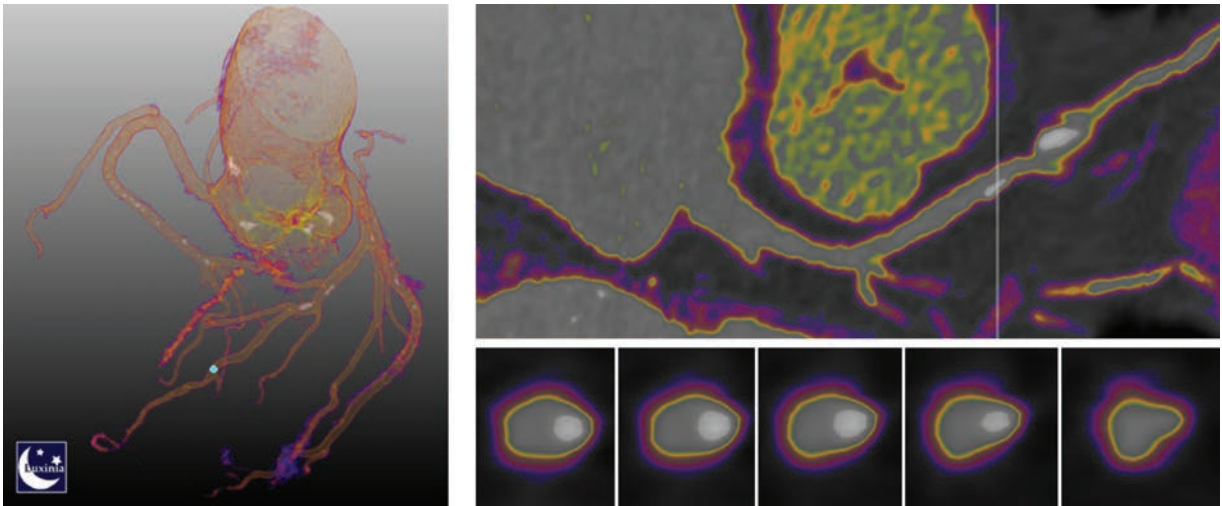


Figure 8: Linked views provided by the prototype application. On the left, the DVR view can be examined by rotating and zooming. The user can pick an arbitrary location, which is masked with a cyan sphere, and the corresponding CPR and oblique MPR views are generated (right). At the bottom right MPR views orthogonal to the local vessel centerline, starting from the white vertical in the CPR view are shown. The prototype enables the user to switch between the conventional gray scale visualization and the TF_{3D} and TF_{2D} based visualizations.

5. Evaluation

We applied our techniques to 12 CTA datasets from a 64-slice MSCT scanner (Siemens Sensation 64). The methods and visualizations were discussed with three board-certified radiologists within the scope of an informal evaluation. All datasets were acquired from living persons. Since no tissue was removed, no histopathological reports were available. Therefore, we focused on the expert's knowledge and the diagnostic evaluation of conventional gray scale views for informal evaluation and discussion of the presented visualizations. For each dataset, the TFs were extracted and a prototype was developed with the MeVisLab platform (www.mevislab.de).

5.1. Visualization environment

The prototype allows for the investigation of the datasets, and contains a DVR view with combined 2D views, consisting of a CPR and an MPR view, see Figure 8. The CPR and MPR view as well as the 3D visualization of the coronary artery tree are linked with each other. On the one hand, the user can traverse the CPR view with the corresponding MPR view being updated. On the other hand, the user can choose an arbitrary vessel segment in the 3D view with the 2D views being generated accordingly.

The evaluation of our prototype included an examination of the DVR views of the coronary artery tree. For comparison, conventional gray scale windowing views were provided. The DVR view allows for overview visualizations of hard plaques and stents, including even smaller hard plaques, see Figure 9. Furthermore, locations of possible stenoses or

pathologic changes of the vessel wall become visible, see Figure 10. Although these changes should be evaluated in more detail in the 2D views, the user can determine interesting coronary artery segments in the 3D view and thus generate CPR and MPR views for the specific locations.

The 2D CPR and MPR views can be evaluated at the same time. Similar to the DVR view, the overview visualization in CPR views of hard plaques and stents were discussed, for example see Figure 11. Again, the TF-based visualizations reveal also smaller hard plaques in comparison to conventional gray scale views. Although stenoses are indicated by the CPR view (see Figure 11), possible findings should be double-checked due to projection-based distortions of the CPR. As shown in Figure 12, the color coding of the vessel wall provides additional information of different accumulations in MPR views. Hence, also hard plaques and stents are highlighted. The presentation of the TF-based visualizations was accompanied with discussions and questions.

5.2. Manipulation of automatically generated TFs

The initial TF_{2D} - and TF_{3D} -based visualizations can be interactively changed to allow for a better exploration of the image data. The user can incrementally modify two offsets. The first offset O_1 defines the relative position of the hard plaque separation, that is S_6 and thus the threshold t , provided in Equation 1. The second one, O_2 , determines the average vessel wall intensity and thus S_3 .

The visualizations of major branches are not impaired, even for strong changes of O_1 , for example 60 HU, see

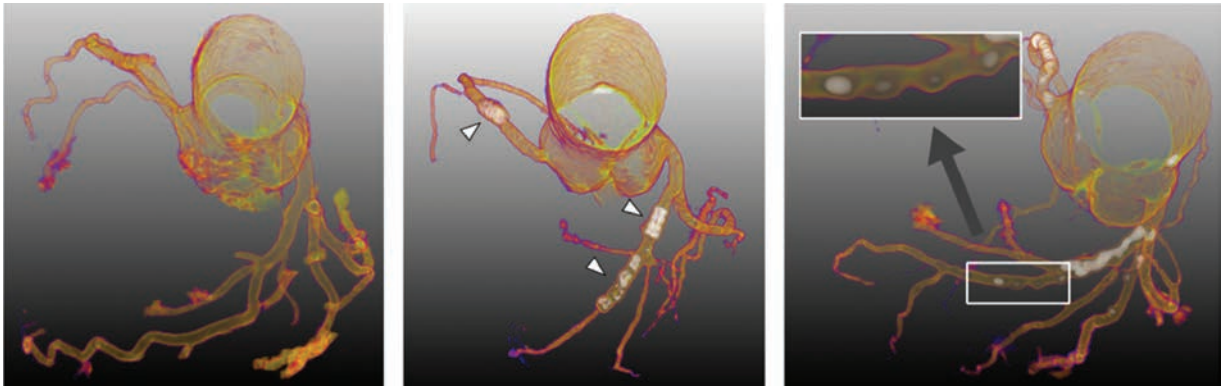


Figure 9: DVR example views of three different datasets. On the left, the DVR view indicates a very low patient's overall plaque burden, since no hard plaques can be seen. The dataset in the middle exhibits three stents (arrowheads), whereas the visualization on the right shows many hard plaques and thus indicates a high overall plaque burden. Even smaller hard plaques are recognizable, see inset.

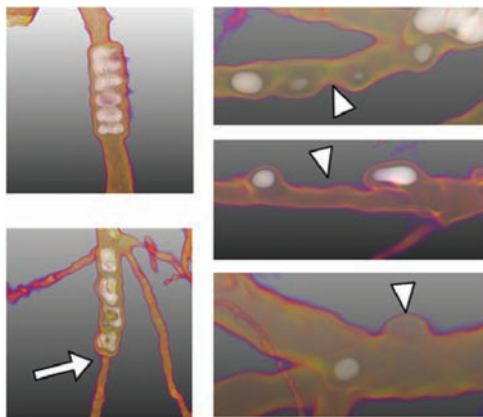


Figure 10: Stenoses of coronary artery vessels in DVR views. On the left, two coronary stents are depicted. The left bottom picture reveals a stenosis (arrow) at the end of the stent, whereas the left upper picture indicates no stenoses. On the right, pathologic changes of the vessel wall lead to positive and negative remodeling (arrowheads). The DVR views provide starting points for further evaluation in 2D views.

Figure 13. For smaller, peripheral branches, contrast agent accumulations or partial volume effect harden the hard plaque separation. In Figure 14, better visualization results can be achieved with an increasing O_1 . With incremental modification of O_1 and extra knowledge about possible positions of hard plaque deposits, that is in the vessel wall and not the lumen, the clinical expert can cope with artefacts in smaller branches.

The modification of O_2 in Figure 15 does not lead to a change in diagnostic evaluation. Larger values for O_2 yield

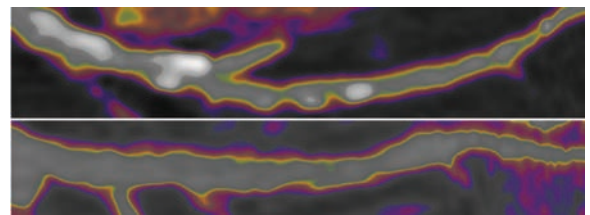


Figure 11: CPR views of the left anterior descending artery of two datasets. The first one (above) exhibits a high hard plaque burden, whereas the second one (below) does not show hard plaque occurrences.

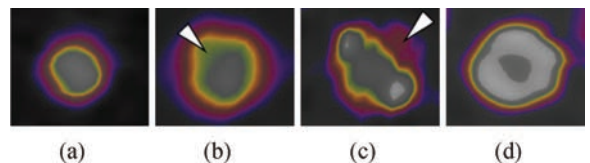


Figure 12: MPR views provide the cross-sectional views of the coronary arteries. The type of the non-calcified plaque (arrowheads) may be inferred from the color coding: MPR view without plaques (a), greenish colors indicate denser structures (b) and pinkish colors indicate lipid accumulations contained in soft plaques (c). In (c), two small hard plaques are highlighted, whereas in (d) a coronary stent is presented.

less highlighting of surrounding tissue, smaller values highlight more of the vessel's environment. However, the vessel's CPR and MPR views with modified TF can still indicate plaque accumulations, see Figure 15.

For diagnostic assessment of plaques, the initial TFs are very robust against changes. For smaller, peripheral branches,

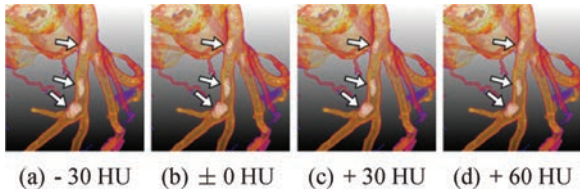


Figure 13: Influence of O_1 for a major branch ($\mu_{blood} = 492HU$, $\sigma_{blood} = 30HU$). In (b) the initial TF reveals some bigger hard plaques (arrows). They are still highlighted, if O_1 is strongly modified, as presented in (a), (c) and (d).

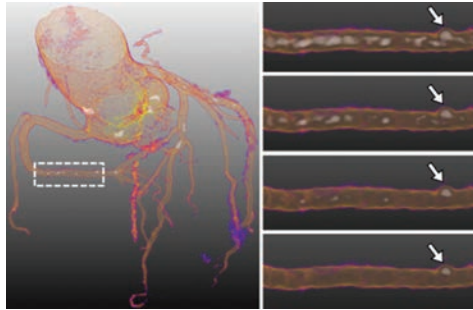


Figure 14: Influence of O_1 for smaller branches similar to Figure 13. From top to bottom, O_1 is assigned with values $-30HU$, $0HU$, $30HU$ and $60HU$. The initial TF (2nd from top) indicate overestimation since it highlights accumulations in the vessel's lumen. Smaller values for O_1 worsen (top), larger values improve (bottom) the result. A small hard plaque is highlighted all the time (arrow).

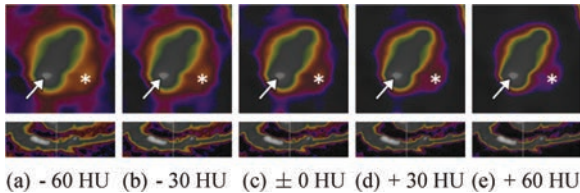


Figure 15: Influence of O_2 . A pathologic vessel wall change (*) as well as a small hard plaque (arrow) is indicated in all visualizations.

artefacts could be reduced with modifications of the automatically generated TFs.

5.3. Feedback of clinical experts

In comparison to the conventional gray scale views with a windowing TF, the clinical experts claim a faster overview of the complex topology, the overall hard plaques and coronary stents, by applying the DVR techniques with the TF_{3D} for the segmented coronary artery tree. With the visual separation

of even small hard plaques in 2D and 3D views, plaque deposits could be analyzed in more detail. Some smaller hard plaques, i.e. with a size of 3 voxels, were not detected with conventional windowing but with a TF_{2D} based view.

The color coding of the vessel wall allows for a qualitative differentiation of vessel wall accumulations. Some cognitive effort was necessary to understand and remember the employed color scale, whereas the assignment of white and beige colors to dense structures like hard plaques and stents was rated to be very intuitive. The opacity mapping of the TF_{3D} provides insight into inner structures. While the 3D view could direct the user's attention to luminal changes, all radiologists pointed out that the evaluation of stenoses requires CPR and MPR views. In the 2D views, the highlighting of the vessel wall was rated high, since indications of possible positive or negative remodeling are provided.

For further improvement, the radiologists claim the combination of our visualization techniques with additional segmentation results to include quantitative parameters, i.e. the vessel lumen or the percent aged vessel lumen's change, since our methods only allow for a qualitative evaluation. A minor drawback concerning the surrounding tissue of hard plaques exists. The surrounding tissue is not highlighted, suggesting the hard plaque is not contained in the vessel wall but in the lumen. Hard plaques are very dense calcium deposits that are surrounded by lipid, fibrous or necrotic accumulations with different intensity values. The HU values of the whole plaque decomposition range from values smaller than the contrast-enhanced blood to values larger than the contrast-enhanced blood. Inherent to 1D TFs, the intermediate intensity values will not be highlighted.

In conclusion, the radiologists prefer the TF-based visualizations in comparison to gray scale views and rate them as useful extension for the evaluation of CTA datasets. The attention is directed to pathologic changes of the vessel wall and thus, the presented techniques allow for a fast qualitative evaluation and detection of the suspicious changes.

However, for clinical decision-making, our approach must be combined with semi-quantitative analyses, where the presented visualizations are combined with quantitative parameters, e.g. the diameter of the vessel's lumen, or a quantitative evaluation of laborious animal studies.

6. Conclusions & Future Work

We presented a method for the visual emphasis and qualitative evaluation of coronary artery plaque. We developed automatically adjusted TFs based on the segmented coronary arteries in CTA image data. The proposed method is also suitable for low quality segmentations, for example with data artefacts or poor contrasts. The plaque deposits consist of different accumulations with different densities. Although an automatic segmentation of all plaque types is not

possible, we present a method for highlighting hard plaques and soft and fibrous plaques by color coding of the vessel wall. Moreover, early stages of the CAD consisting of non-stenotic plaque deposits can be visualized.

The adapted TFs were combined with common visualization techniques of CTA datasets. An informal evaluation with three radiologists rates our methods as beneficial extensions for conventional CTA evaluation. Due to the locally non-uniform spatial diffusion of the contrast medium the presented approach could be the basis for a more sophisticated uncertainty visualization, as presented by [LLPY07]. In addition, size-based TFs as employed in [CM08] could be applied and compared to the presented approach.

Problems arose due to the non-uniform spatial variation of the contrast medium that resulted in different contrast agent accumulations. Because we experienced a loss of quality for vessel wall intensity approximation for smaller branches with too few voxels for a reliable local histogram analysis via IPV extraction, we employed a global TF. A higher spatial resolution of the image data would be required to enable a successful local TF adaption.

Further improvements might also be possible with more advanced segmentation methods. As an example, the approach developed by Friman *et al.* [FHP 08] is promising since it provides subvoxel accuracy for centerline extraction of segmented vessels. Considering the highlighting of coronary stents, the segmentation of stents during preprocessing could improve the CTA visualization.

Acknowledgements

We thank Dr. S. Achenbach (University of Erlangen-Nürnberg) for providing the image data and Fraunhofer MEVIS for advanced MeVisLab features.

References

- [AJH*90] AGATSTON A. S., JANOWITZ W. R., HILDNER F., ZUSMER N. R., VIAMONTE M. J., DETRANO R.: Quantification of coronary artery calcium using ultrafast computed tomography. *Journal of American College of Cardiology* 15, 4 (1990), 827–832.
- [Ame07] AMERICAN HEART ASSOCIATION: Heart Disease and Stroke Statistics—2007 Upd. *Circulation* 115, (2007), e69–171.
- [BA02] BULLITT E., AYLWARD S. R.: Volume rendering of segmented image objects. *IEEE Transactions on Medical Imaging* 21, 8 (2002), 998–1002.
- [BG09] BRUCKNER S., GRÖLLER M.: Instant Volume Visualization using Maximum Intensity Difference Accumulation. *Computer Graphics Forum* 28, 3 (2009), 775–882.
- [CM08] CORREA C. D., MA K.-L.: Size-based Transfer Functions: A New Volume Exploration Technique. *IEEE Transactions on Visualization and Computer Graphics* 14, 6 (2008), 1380–1387.
- [EKE01] ENGEL K., KRAUS M., ERTL T.: High-quality pre-integrated volume rendering using hardware-accelerated pixel shading. In *Proceedings of the ACM SIGGRAPH/EUROGRAPHICS Workshop on Graphics Hardware* (New York, NY, USA, 2001), ACM, pp. 9–16.
- [FDHL03] FERCHER A. F., DREXLER W., HITZENBERGER C. K., LASSER T.: Optical Coherence Tomography—Principles and Applications. *Reports on Progress in Physics* 66, (2003), 239–303.
- [FHP08] FRIMAN O., HINDENNACH M., PEITGEN H.-O.: Template-based multiple hypotheses tracking of small vessels. In *Proceedings of IEEE 5th International Symposium on Biomedical Imaging (ISBI'08)* (Paris, France, 2008), IEEE Computer Society, pp. 1047–1050.
- [HBF*05] HENNEMUTH A., BOSKAMP T., FRITZ D., KÜHNEL C., BOCK S., RINCK D., *et al.*: One-click coronary tree segmentation in CT angiographic images. *CARS'05: Computer Assisted Radiology and Surgery* 1281, (2005), 317–321.
- [HBS*02] HONG C., BECKER C. R., SCHOEPF U. J., *et al.*: Coronary Artery Calcium: Absolute Quantification in Nonenhanced and Contrastenhanced Multi-Detector Row CT Studies. *Radiology* 223, (2002), 474–480.
- [HZZ*07] HERZOG C., ZANGOS S., ZWERNER P., COSTELLO P., VOGL T. J., SCHOEPF J. U.: CT of Coronary Artery Disease. *Journal of Thoracic Imaging* 22, 1 (2007), 40–48.
- [IRvG07] ISGUM A., RUTTEN A., VAN GINNEKEN B.: Detection of coronary calcifications from computed tomography scans for automatic risk assessment of coronary artery disease. *Medical Physics* 34, 4 (2007), 1450–1461.
- [JQD*08] JOSHI A., QIAN X., DIONE D. P., BULSARA K. R., BREUER C. K., SINUSAS A. J., PAPADEMETRIS X.: Effective visualization of complex vascular structures using a non-parametric vessel detection method. *IEEE Transactions on Visualization and Computer Graphics* 14, 6 (2008), 1603–1610.
- [KFW*02] KANITSAR A., FLEISCHMANN D., WEGENKITTL R., FELKEL P., GRÖLLER M. E.: Cpr: curved planar reformation. In *VIS '02: Proceedings of the Conference on Visualization '02* (Washington, DC, USA, 2002), IEEE Computer Society, pp. 37–44.
- [KHB*06] KUEHNEL C., HENNEMUTH A., BOCK S., OELTZE S., BOSKAMP T., KRASS S., *et al.*: New Software Assistants for Cardiovascular Diagnosis. In *GI-Workshop "Softwareassistenten—Computerunterstützung für die*

medizinische Diagnose und Therapieplanung" within the GI annual conference (2006), Gesellschaft für Informatik, Bonn, Germany, pp. 491–498.

- [KKH02] KNISS J., KINDLMANN G., HANSEN C.: Multidimensional Transfer Functions for Interactive Volume Rendering. *IEEE Transactions on Visualization and Computer Graphics* 8, 3 (2002), 270–285.
- [LLPY07] LUNDSTRÖM C., LJUNG P., PERSSON A., YNNERMAN A.: Uncertainty visualization in medical volume rendering using probabilistic animation. *IEEE Transactions on Visualization and Computer Graphics* 13, 6 (2007), 1648–1655.
- [LLY05] LUNDSTRÖM C., LJUNG P., YNNERMAN A.: Extending and simplifying transfer function design in medical volume rendering using local histograms. In *EUROVIS 2005: Eurographics/IEEE VGTC Symposium on Visualization* (Leeds, United Kingdom, 2005), Eurographics Association, pp. 263–270.
- [NRJ93] NAPEL S., RUBIN G. D., JEFFREY R. B. J.: STS-MIP: a new reconstruction technique for CT of the chest. *Journal of Computer Assisted Tomography* 17, 5 (1993), 832–838.
- [PAM*07] POHLE K., ACHENBACH S., MACNEILL B., ROPERS D., FERENCIK M., et al.: Characterization of non-calcified coronary atherosclerotic plaque by multi-detector row CT: Comparison to IVUS. *Atherosclerosis* 190 (2007), 174–180.
- [PO07] PREIM B., OELTZE S.: *Visualization in medicine and life sciences. 3D Visualization of Vasculature: An Overview* (New York, NY, USA, 2007), Springer-Verlag, pp. 19–39.
- [RSK06] REZK-SALAMA C., KOLB A.: Opacity Peeling for Direct Volume Rendering. *IEEE/Eurographics Symposium on Visualization* 25, 3 (2006), 597–606.
- [SCC*04] STRAKA M., CERVENANSKY M., CRUZ A. L., KOCHL A., SRAMEK M., GRÖLLER E., FLEISCHMANN D.: The Vessel Glyph: Focus & context visualization in CT-angiography. In *Proceedings of VIS '04: Proceedings of the Conference on Visualization '04* (Washington, DC, USA, 2004), IEEE Computer Society, pp. 385–392.
- [SHN*06] SCHARSACH H., HADWIGER M., NEUBAUER A., WOLFSBERGER S., BÜHLER K.: Perspective Isosurface and direct volume rendering for virtual endoscopy applications. In *EUROVIS—Eurographics/IEEE VGTC Symposium on Visualization* (Lisbon, Portugal, 2006), Eurographics Association, pp. 315–322.
- [SPSP02] SELLE D., PREIM B., SCHENK A., PEITGEN H.-O.: Analysis of vasculature for liver surgical planning. *IEEE Transactions on Medical Imaging* 21, 11 (2002), 1344–1357.
- [TPD06] TAPPENBECK A., PREIM B., DICKEN V.: Distance-based transfer function design: specification methods and applications. In *Simulation und Visualisierung* (2006), SCS, Erlangen, Germany, pp. 259–274.
- [vOVGR*03] VAN OOIJEN P. M. A., VAN GEUNS R. J. M., RENSING B. J. W. M., BONGAERTS A. H. H., et al.: Non-invasive coronary imaging using electron beam CT: surface rendering versus volume rendering. *AJR* 180 (2003), 223–226.
- [VST*03] VEGA F., SAUBER N., TOMANDL B., NIMSKY C., GREINER G., HASTREITER P.: Enhanced 3D-Visualization of intracranial aneurysms involving the skull base. In *Proceedings of MICCAI* (New York, NY, USA, 2003), vol. 2879, LNCS, Springer-Verlag, pp. 256–263.
- [VST*04] VEGA HIGUERA F., SAUBER N., TOMANDL B., NIMSKY C., et al.: Automatic adjustment of bidimensional transfer functions for direct volume visualization of intracranial aneurysms. In *Proceedings of SPIE Conference on Medical Image Computing* (2004), vol. 5367, SPIE The International Society for Optical Engineering, Bellingham, USA, pp. 275–284.
- [WFKF06] WESARG S., FAWAD KHAN M., FIRLE E.: Localizing calcifications in cardiac CT data sets using a new vessel segmentation approach. *Journal of Digit Imaging* 19, 3 (2006), 249–257.